Link Performance of Multiple Reconfigurable Intelligent Surfaces and Direct Path in General Fading

Islam M. Tanash and Taneli Riihonen
Faculty of Information Technology and Communication Sciences, Tampere University, Finland
e-mail: {islam.tanash, taneli.riihonen}@tuni.fi

***Abstract*—We analyze the performance of a single-input single-output wireless link that is aided by multiple reconfigurable intelligent surfaces (RISs) — in terms of outage probability, average symbol error probability and ergodic capacity, for which we derive analytical expressions in closed form. In particular, we consider a realistic system model, where the direct path may not be blocked and for which channels corresponding to different RISs are assumed to be independent but not identical and follow the generic κ-μ fading distribution, which can be reduced to a number of fading scenarios (namely Rayleigh, Rice, Nakagami-m, and one-sided Gaussian). This enables the evaluation of the system performance when adopting any combination of these special cases or the generic κ-μ distribution for both hops of the multiple distributed RISs. The direct path is modeled by Rayleigh fading assuming no line-of-sight between the source and the destination. We verify the accuracy of the adopted approach by means of Monte Carlo simulations and conduct a performance analysis that demonstrates the significant improvement in the system performance due to the usage of the RISs. Especially, we show that increasing the number of reflecting elements equipped on the RISs and placing the RISs closer to either communication endpoints improve the performance considerably.**

I. Introduction

The reconfigurable intelligent surface (RIS) is a promising emerging technology for future wireless communication networks since it gives more control over the wireless environment for the aim of improving the quality-of-service and spectrum efficiency. It consists of a large surface that has low-cost passive reflecting elements (REs) that can be adapted by a microcontroller to collaboratively reflect the incident electromagnetic signals into the desired direction.

Most of the research work conducted on this topic focuses on the design [1], [2], optimization [3]–[5] and potential applications [6]–[8] of RIS-aided systems. Specifically, in [1], a digitally controlled metasurface, whose units can be adapted independently, is designed to dynamically manipulate the electromagnetic waves and, thus, achieve more versatility; whereas in [2], a tunable metasurface is designed to work as a spatial microwave modulator with energy feedback.

Prior works have also investigated optimizing the performance of RIS-aided wireless systems: In [3], the authors solve a non-convex optimization problem to maximize their system's energy efficiency; and in [4], the discrete phase shifts together with the transmit beamforming of a multiantenna base station are optimized to minimize transmission power. In addition, the authors in [5], who adopt RISs at the edge of cells to enhance the downlink transmission for cell-edge users, aim toward maximizing the weighted sum rate of all users by optimizing the transmitter's active precoding matrices together with the REs' phase shifts.

The applications of RISs span the different areas of wireless communications, where it is adopted in [6] to support the communication in unmanned aerial vehicle-assisted wireless systems and in [7] to assist the data transmission from a base station to a single-antenna receiver in an RIS-assisted millimeter wave system. The RIS technology can also be adopted in wireless networks to enhance the physical layer security as explained in [8]. On the other hand, the theoretical study of RIS-aided wireless networks still in its early stage, where limited number of research works have been established to analyze the performance of these systems due to the difficulty in evaluating the statistical characterization of the end-to-end signal-to-noise ratio (SNR). Therefore, several approximations, bounds or asymptotic analysis have been developed to analyze the RIS-aided systems [9], [10].

Noticeable efforts have been made on studying the generic single-input single-output (SISO) system model without direct path, where the central limit theorem (CLT) is used to derive bounds or approximations for the different performance measures for Rayleigh distribution in [11], [12]. A different approximating approach is used in [13], [14] to achieve high accuracy regardless of the number of REs at the RIS. The SISO system with Rician fading and direct path between the source (S) and destination (D) is studied in [15], for which the statistical characterization of the end-to-end SNR is not evaluated and thus the symbol error rate is not derived either.

A more generic SISO system with multiple RISs is investigated in [16], [17] and different approaches are used to approximate the channel statistics. All the fading channels associated with different RISs are assumed to be independent and identically distributed (i.i.d.). However, this does not represent a realistic assumption since the RISs may be distributed over a wide geographical area. Therefore, different RISs are expected to experience non-identical channels of the same or different fading distribution. On the other hand, for each RIS, the channels encountered by REs can be assumed to be i.i.d. since they are placed on the same surface, i.e., the REs of a single RIS are located very close to each other.

Motivated by the fact that the literature only considers the case where the same fading model is assumed for both hops (S–RIS and RIS–D) among all the distributed RISs and with i.i.d. channels, we present herein a more realistic performance study of a generic SISO system model with multiple RISs and direct path with independently but non-identically distributed (i.n.i.d.) fading channels across the distributed RISs which are geographically far apart from each other, and thus each RIS may also experience different fading distribution. Therefore, we choose to evaluate the system's performance over the generic κ-μ distribution which can be reduced to a number of the most used fading scenarios, namely, Rayleigh, Rice, Nakagami-m and one-sided Gaussian distribution. This allows us not only to consider the same double fading channels for all the distributed RISs, but also to consider different combinations of the special cases or the generic distribution for the S–RIS and RIS–D links of the different RISs.

In particular, we implement the Laguerre series method [18] to approximate the statistical characterization of the end-to-end equivalent channel of the SISO system with multiple RISs and direct path. Closed-form expressions for the outage probability and ergodic capacity are presented as well as a novel expression for the average symbol error probability (ASEP) is derived. Our work presents generalized results that are valid for any number of RISs equipped with arbitrary numbers of REs. It is also valid for any combination of the fading distributions covered by the κ-μ distribution and with or without direct path, where the latter represents a special case of the former when the direct channel gain is set to zero.

II. System and Channel Models

The system under study is illustrated in Fig. 1 and it consists of a single-antenna source (S), N RISs, where the nth one (RIS$_n$) is equipped with M_n REs, and a single-antenna destination (D). The destination can overhear the signal from all the distributed RISs as well as through the direct path. It is worth mentioning that the considered system model includes the special case of an obstructed direct path between S and D, for which the channel coefficient u below in (2) equals zero.

A. Signal Models

The received signal at the destination can be written as

$$y = A\, s + w, \tag{1}$$

for which the combined channel response is

$$A = \sum_{n=1}^{N} A_n + u, \tag{2}$$

where the channel response of the nth RIS is

$$A_n = \sum_{i=1}^{M_n} h_{n,i}\, g_{n,i}\, r_{n,i}, \tag{3}$$

and s is the transmitted signal, $h_{n,i}$, $g_{n,i}$ and u are the fading coefficients of S–RIS$_n$, RIS$_n$–D and S–D links, respectively, while the additive white Gaussian noise is denoted by w in (1)

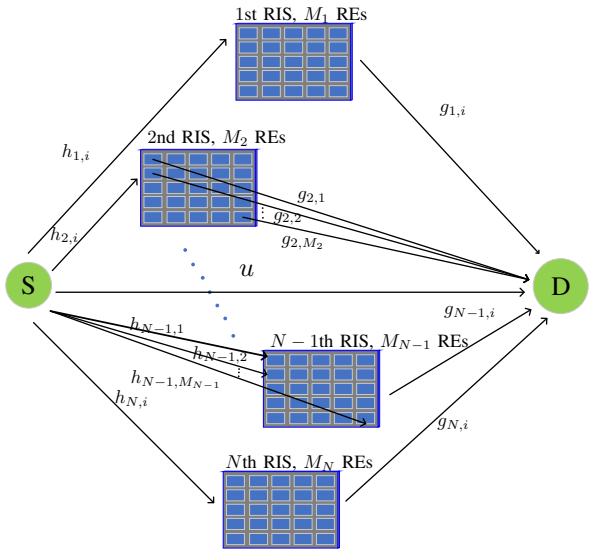

Fig. 1. A SISO wireless system with N RISs. Each S–RIS$_n$ and RIS$_n$–D path consists of multiple propagation paths through the M_n REs. For simplicity, we illustrate the multipath components via two RISs only.

with zero mean and variance $N_0 = \mathrm{E}[|w|^2]$. The instantaneous end-to-end SNR is defined as $\rho = E_s\,|A|^2/N_0 = \rho_0\,|A|^2$ with $E_s = \mathrm{E}[|s|^2]$ being the transmitted power and $\rho_0 = E_s/N_0$ denoting the transmit SNR. In addition, $r_{n,i} = \exp(j\theta_{n,i})$ is the response of the ith RE in the nth RIS for which its magnitude is assumed to be equal to one and its phase shift is optimized to maximize the SNR at the receiver by choosing $\theta_{n,i} = \angle u - \left(\angle h_{n,i} + \angle g_{n,i}\right)$, assuming ideal global channel state information and centralized coordination.

B. Fading Models

The flat fading coefficients $h_{n,i}$, $g_{n,i}$ and u are assumed to be statistically independent, identical per RIS, and slowly varying. On the other hand, they are not identical for the different RISs, which are geographically separated far apart from each other. The average gains of their envelopes are defined respectively as $\sigma^2_{h_n} = \mathrm{E}\left[|h_{n,i}|^2\right] = \iota_0\,(\frac{d_0}{d_{h_n}})^{\eta_{h_n}}$, $\sigma^2_{g_n} = \mathrm{E}\left[|g_{n,i}|^2\right] = \iota_0\,(\frac{d_0}{d_{g_n}})^{\eta_{g_n}}$ and $\sigma^2_u = \mathrm{E}\left[|u|^2\right] = \iota_0\,(\frac{d_0}{d_u})^{\eta_u}$, where ι_0 is the reference path loss at the reference distance d_0, and d_j and η_j, $j \in \{h_n, g_n, u\}$ denote respectively the distance and path loss exponent of the corresponding link. We let $|h_{n,i}|$ and $|g_{n,i}|$ follow generalized κ-μ fading distribution, for which κ is the ratio between the total power of the dominant components and the total power of the scattered waves, and μ is the number of multipath clusters [19]. Assuming there is no line-of-sight (LoS) in the direct path, the S–D link can be modeled by Rayleigh fading.

The κ-μ distribution encloses most of common small-scale fading models as special cases that are obtained by controlling the values of its fading parameters. In particular, for Rayleigh ($\kappa = 0, \mu = 1$), Nakagami-m ($\kappa = 0, \mu = m$), Rice ($\kappa = K, \mu = 1$) and one-sided Gaussian ($\kappa = 0, \mu = 0.5$), where m and K refer respectively to the shape parameter of the

Nakagami-m distribution and to the Rician factor. Therefore, in addition to the generic κ-μ distribution, we can consider the same or combination of the special-case distributions for both links of the N distributed RISs by assigning the corresponding values to κ_{h_n} and μ_{h_n} of the S–RIS$_n$ hop and to $\kappa_{g,n}$ and $\mu_{g,n}$ of the RIS$_n$–D hop.

Toward evaluating the performance measures of the considered system, we need to derive the probability density function (PDF) of the end-to-end SNR for the system under study. We achieve that by first deriving the PDF and the cumulative distribution function (CDF) of the combined channel response defined in (2). It is obvious that the channel response of the nth RIS defined in (3) is a sum of M_n identical double κ-μ random variables, which all are continuous, independent and defined over the positive real axis. Therefore, their sum converges toward a normal random variable according to the central limit theorem. As a result, the combined channel response, which is a sum of the N resulted normal variables plus a single Rayleigh random variable will also be nearly normally distributed and its PDF will look similar to the Gaussian PDF with a single maximum, and its tails extend to infinity from the right side but is truncated to zero from the left side.

The PDF of the combined nearly-Gaussian channel response can be further tightly approximated by the first term of a Laguerre series expansion as stated in [18] as

$$f_{|A|}(x) \simeq \frac{x^{\alpha}}{\beta^{\alpha+1}\,\Gamma(\alpha+1)}\,\exp\left(-\frac{x}{\beta}\right), \tag{4}$$

where

$$\alpha = \frac{(\mathrm{E}[|A|])^2}{\mathrm{Var}[|A|]} - 1, \tag{5}$$

$$\beta = \frac{\mathrm{Var}[|A|]}{\mathrm{E}[|A|]}. \tag{6}$$

The corresponding CDF can be derived [13, Appendix A] as

$$F_{|A|}(x) \simeq \frac{\gamma\left(\alpha+1, x/\beta\right)}{\Gamma(\alpha+1)}, \tag{7}$$

where $\gamma(\cdot,\cdot)$ denotes the lower incomplete Gamma function.

The mean of $|A|$ is calculated using its linearity property together with the independency assumption as $\mathrm{E}[|A|] = \sum_{n=1}^{N}\mathrm{E}[|A_n|]+\mathrm{E}[|u|] = \sum_{n=1}^{N} M_n\ \mathrm{E}[|h_{n,i}|]\,\mathrm{E}[|g_{n,i}|]+\mathrm{E}[|u|]$ for which the expectation of a κ-μ distributed fading coefficient is given in [20, Eq. 3] and the cth moment of a Rayleigh-distributed fading coefficient is $\mathrm{E}[|u|^c] = \sigma_u^c\,\Gamma\left(1+\frac{c}{2}\right)$. Therefore,

$$\begin{aligned}\mathrm{E}[|A|] = \sum_{n=1}^{N} M_n\, &\frac{\sigma_{h_n}\,\Gamma\left(\mu_{h_n}+\frac{1}{2}\right)\,\exp(-\kappa_{h_n}\,\mu_{h_n})}{\Gamma(\mu_{h_n})\,((1+\kappa_{h_n})\,\mu_{h_n})^{\frac{1}{2}}}\\ &\times \frac{\sigma_{g_n}\,\Gamma\left(\mu_{g_n}+\frac{1}{2}\right)\,\exp(-\kappa_{g_n}\,\mu_{g_n})}{\Gamma(\mu_{g_n})\,((1+\kappa_{g_n})\,\mu_{g_n})^{\frac{1}{2}}}\\ &\times {}_1F_1(\mu_{h_n}+\frac{1}{2};\mu_{h_n};\kappa_{h_n}\,\mu_{h_n})\\ &\times {}_1F_1(\mu_{g_n}+\frac{1}{2};\mu_{g_n};\kappa_{g_n}\,\mu_{g_n}) + \sqrt{\frac{\pi\,\sigma_u^2}{4}},\end{aligned} \tag{8}$$

where ${}_1F_1(\cdot;\cdot;\cdot)$ is the confluent hypergeometric function of the first kind [21, Eq. 9.210.1].

Likewise, the variance of $|A|$ is calculated as $\mathrm{Var}[|A|] = \sum_{n=1}^{N}\mathrm{Var}[|A_n|] + \mathrm{Var}[|u|]$, where

$$\begin{aligned}\mathrm{Var}[|A_n|] &= M_n\ \mathrm{Var}[|h_{n,i}\,g_{n,i}|]\\ &= M_n\,(\mathrm{E}[|h_{n,i}|^2]\,E[|g_{n,i}|^2] - \mathrm{E}[|h_{n,i}|]^2\ \mathrm{E}[|g_{n,i}|]^2)\end{aligned} \tag{9}$$

and $\mathrm{Var}[|u|] = \mathrm{E}[|u|^2]-(\mathrm{E}[|u|])^2$, which leads us to evaluating it as shown in (10) at the top of the next page.

Finally, we can derive the PDF of the end-to-end SNR by taking the derivative of the CDF of ρ that is defined as

$$F_{\rho}(x) = \Pr(\rho \le x) = F_{|A|}\left(\sqrt{\frac{x}{\rho_0}}\right). \tag{11}$$

Therefore,

$$f_{\rho}(x) \simeq \frac{1}{2\,\beta^{\alpha+1}\,\Gamma(\alpha+1)}\,\rho_0^{-\frac{\alpha+1}{2}}\,x^{\frac{\alpha-1}{2}}\,\exp\left(-\sqrt{\frac{x}{\beta^2\,\rho_0}}\right). \tag{12}$$

III. Performance Analysis

The performance of the considered system is studied in this section in terms of three central performance metrics, namely outage probability, ASEP and ergodic capacity.

The outage probability that is defined as the probability that the end-to-end instantaneous SNR falls below a predefined threshold value, ρ_{th}, is given directly [13, Eq. 31] by

$$P_O = F_{\rho}(\rho_{th}) \simeq \frac{\gamma\left(\alpha+1, \frac{1}{\beta}\sqrt{\frac{\rho_{th}}{\rho_0}}\right)}{\Gamma(\alpha+1)}. \tag{13}$$

The average symbol error probability (ASEP) under fading for coherent detection is obtained in most cases by evaluating

$$\bar{P}_E = \int_0^{\infty} \Omega\left(Q\left(\sqrt{\zeta\,x}\right)\right)\,f_{\rho}(x)\,\mathrm{d}x, \tag{14}$$

where $\Omega(\cdot)$ is some polynomial of the Q-function that corresponds to the conditional error probability, e.g.,

$$\begin{aligned}\Omega\left(Q\left(\sqrt{\zeta\,x}\right)\right) = 4\left(\frac{\sqrt{\mathcal{M}}-1}{\sqrt{\mathcal{M}}}\right)Q\left(\sqrt{\zeta\,x}\right)\\ - 4\left(\frac{\sqrt{\mathcal{M}}-1}{\sqrt{\mathcal{M}}}\right)^2 Q^2\left(\sqrt{\zeta\,x}\right)\end{aligned} \tag{15}$$

for square $\mathcal{M}$-quadrature amplitude modulation ($\mathcal{M}$-QAM) [22], whereas the constant $\zeta = \frac{3}{\mathcal{M}-1}$. We can derive a closed-form expression for (14) by substituting the exponential approximation proposed in [23] into the above integral as

$$\bar{P}_E = \sum_{r=1}^{R} a_r \int_0^{\infty} \exp(-b_r\,\zeta\,x)\,f_{\rho}(x)\,\mathrm{d}x, \tag{16}$$

where $\{(a_r, b_r)\}_{r=1}^{R}$ is some set of coefficients from [24]. The above expression is presented with an equality because there is practically no approximation error in the present application despite its being an approximation in the strict sense.

$$\mathrm{Var}[|A|] = \sum_{n=1}^{N} M_n \Bigg(\sigma_{h_n}^2 \, \sigma_{g_n}^2 - \frac{\sigma_{h_n}^2 \, \Gamma^2\left(\mu_{h_n} + \frac{1}{2}\right) \exp(-2\,\kappa_{h_n}\,\mu_{h_n})}{\Gamma^2(\mu_{h_n})\,(1+\kappa_{h_n})\,\mu_{h_n}} \frac{\sigma_{g_n}^2 \, \Gamma^2\left(\mu_{g_n} + \frac{1}{2}\right) \exp(-2\,\kappa_{g_n}\,\mu_{g_n})}{\Gamma^2(\mu_{g_n})\,(1+\kappa_{g_n})\,\mu_{g_n}} \times {}_1F_1^2(\mu_{h_n} + \frac{1}{2}; \mu_{h_n}; \kappa_{h_n}\,\mu_{h_n})\, {}_1F_1^2(\mu_{g_n} + \frac{1}{2}; \mu_{g_n}; \kappa_{g_n}\,\mu_{g_n}) \Bigg) + \frac{4-\pi}{4}\,\sigma_u^2 \tag{10}$$

$$\bar{\mathcal{C}} \simeq \frac{1}{\ln(2)\,\Gamma(\alpha+1)} \Bigg(\frac{\Gamma(\alpha-1)\,{}_2F_3\left(1,1;2,1-\frac{\alpha}{2},\frac{3}{2}-\frac{\alpha}{2};-\frac{1}{4\beta^2\rho_0}\right)}{\beta^2\rho_0} + \frac{\pi\,\beta^{-\alpha-2}\,\rho_0^{-\frac{\alpha}{2}-1}\csc\left(\frac{\pi\alpha}{2}\right)\,{}_1F_2\left(\frac{\alpha}{2}+1;\frac{3}{2},\frac{\alpha}{2}+2;-\frac{1}{4\beta^2\rho_0}\right)}{\alpha+2} + \frac{\pi\,\beta^{-\alpha-1}\,\rho_0^{-\frac{\alpha}{2}-\frac{1}{2}}\sec\left(\frac{\pi\alpha}{2}\right)\,{}_1F_2\left(\frac{\alpha}{2}+\frac{1}{2};\frac{1}{2},\frac{\alpha}{2}+\frac{3}{2};-\frac{1}{4\beta^2\rho_0}\right)}{\alpha+1} - 2\,\alpha^2\,\Gamma(\alpha-1)\,\ln\left(\frac{1}{\beta\sqrt{\rho_0}}\right) + 2\,\alpha\,\Gamma(\alpha-1)\,\ln\left(\frac{1}{\beta\sqrt{\rho_0}}\right) + 2\,(\alpha-1)\,\alpha\,\Gamma(\alpha-1)\,\psi^{(0)}(\alpha+1) \Bigg) \tag{18}$$

By substituting (12) in (16) and using [21, Eq. 3.462.1], we obtain

$$\bar{P}_E = \frac{1}{2\,\beta^{\alpha+1}\,\Gamma(\alpha+1)} \sum_{r=1}^{R} a_r \, (\rho_0\,\zeta\,b_r)^{-\frac{\alpha+1}{2}} \Bigg(\Gamma\left(\frac{\alpha+1}{2}\right) \times {}_1F_1\left(\frac{\alpha+1}{2},\frac{1}{2},\frac{1}{4\,\beta^2\,\rho_0\,\zeta\,b_r}\right) - \left(\beta^2\,\rho_0\,\zeta\,b_r\right)^{-\frac{1}{2}} \times \Gamma\left(\frac{\alpha}{2}+1\right)\,{}_1F_1\left(\frac{\alpha}{2}+1,\frac{3}{2},\frac{1}{4\,\beta^2\,\rho_0\,\zeta\,b_r}\right) \Bigg), \tag{17}$$

for which α and β are defined respectively in (5) and (6).

The ergodic capacity of the considered system has the same analytical form as [14, Eq. 11] that is rewritten in (18) with substituting novel expressions of α and β, which are calculated herein using the mean and variance of the combined channel response in (8) and (10), respectively. The $\psi^{(0)}(\cdot)$ in (18) is the 0th polygamma function and $\csc(\cdot)$ is the cosecant function.

IV. Numerical Results and Discussions

This section gives insight into the performance of the considered system in terms of the outage probability, ASEP and ergodic capacity. In addition, it verifies the accuracy of the adopted Laguerre series approximation by means of Monte Carlo simulations. We assume five different RISs ($N = 5$) whose number of REs is given as $\{M_n\}_{n=1}^{N} = \{14, 26, 16, 24, 20\}$ or $\{M_n\}_{n=1}^{N} = \{28, 52, 32, 48, 40\}$. Also, M refers to the total number of REs in all the N distributed RISs, i.e., $M = \sum_{n=1}^{N} M_n$. Thus, $M = 100$ and $M = 200$ for the two considered cases. For calculating the average gains $\sigma_{h_n}^2, \sigma_{g_n}^2, \sigma_u^2$, we set $d_0 = 1$ m, $\iota_0 = -30$ dB, $\eta_{h_n} = 2.4, \eta_{g_n} = 2.3$ for all $n = 1, 2, \ldots, 5$ and $\eta_u = 3$. The RISs are assumed to be distributed between S and D which are located in the x-axis and separated by a distance $d_u = 100$ m. The location of each RIS is given in the Cartesian coordinate system as (d_{x_n}, d_{y_n}) and the total distances of the links are calculated as $d_{h_n} = \sqrt{d_{x_n}^2 + d_{y_n}^2}$ and $d_{g_n} = \sqrt{(d_u - d_{x_n})^2 + d_{y_n}^2}$.

Unless otherwise stated, we consider the location setting $D = [(25, 50), (40, 30), (55, 10), (82, -20), (95, -40)]$ m and S–RIS$_n$–D paths' distributions with
$\kappa_{h_1} = 0, \mu_{h_1} = 1, \kappa_{g_1} = 0, \mu_{g_1} = 1$ (double Rayleigh),
$\kappa_{h_2} = 0, \mu_{h_2} = 3, \kappa_{g_2} = 0, \mu_{g_2} = 2$ (double Nakagami),
$\kappa_{h_3} = 2, \mu_{h_3} = 1, \kappa_{g_3} = 2, \mu_{g_3} = 1$ (double Rician),
$\kappa_{h_4} = 1, \mu_{h_4} = 2, \kappa_{g_4} = 1, \mu_{g_4} = 2$ (double $\kappa - \mu$), and
$\kappa_{h_5} = 2.5, \mu_{h_5} = 1, \kappa_{g_5} = 0, \mu_{g_5} = 3.3$ (Rician–Nakagami).

The accuracy of the first-term Laguerre approximation (4) for the end-to-end channel's PDF of the considered system model with and without direct path between S and D is tested and illustrated in Fig. 2. It can be noted that the used approximation is very tight for both communication scenarios (with or without direct path) and for any combination of the fading distributions, where we verified its accuracy over two fading scenarios; all links experience Rician fading or each RIS experiences different fading distribution using the setting specified above. The high accuracy is maintained for low and high numbers of the RISs' REs. The communication scenario, where only a S–D link exist, is also presented for comparison and it shows that imposing the RISs in the system increases its power gain which increases even further by increasing M as can be depicted from the right-shifting of the PDF.

Figure 3 depicts the impact of using RISs to assist the communication between S and D and enhance the different performance metrics. In particular, the outage probability, ASEP and the ergodic capacity, whose analytical values coincide well with the true measures, show much better performance when compared to the scenario where communication is achieved only through the direct path. In addition, the impact of increasing the number of REs equipped on the distributed RISs is clearly noted where as M increases, the outage probability and ASEP decrease and the ergodic capacity increases, indicating improved performance, i.e., less transmitted power is required

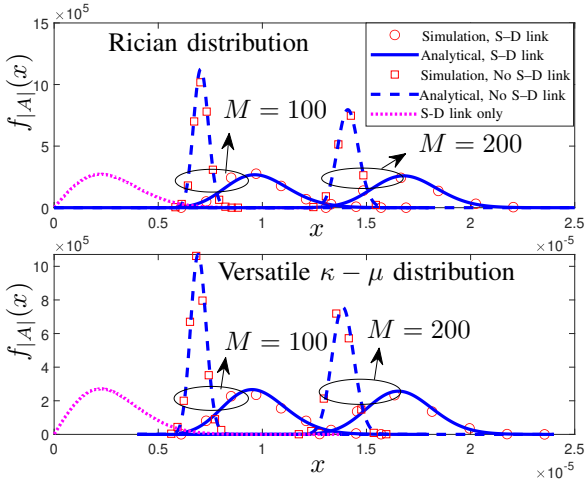

Fig. 2. The PDF of the end-to-end channel with and without S–D link for $N = 5$ of two different RISs systems.

to achieve a certain level of the considered measure.

The effect of increasing M on the different orders of the considered $\mathcal{M}$-QAM scheme in Fig. 3(b) is nearly the same, e.g., for ASEP of 10%, an increment by 100 REs will decrease the required transmitted power by approximately 2.2 dB for both schemes. Moreover, it can be noted from Fig. 3(a) and (b), that as M increases, the rate of change in the slope of the outage probability and the ASEP increases which indicates higher diversity gain.

Finally, we demonstrate the impact of the locations of the N distributed RISs to the system's performance. To give a better insight into it, we test the x-position and the y-position separately, while keeping the other dimension's position constant. In particular, in Fig. 4(a), we choose three different location settings for the five distributed RISs as indicated by the three different marker symbols in the smaller subfigure to represent the different possibilities of movements along the x-axis. The corresponding ASEP is calculated and plotted. We conclude from the figure that as the x-position of the RISs is nearer to either S or D, better performance is achieved. On the other hand, placing the RISs near the half-way between S and D results in worse performance since the path losses for both hops are maximized. Similarly, the y-placement of the RISs is also tested in Fig. 4(b) and shows better performance when the RISs are placed vertically closer to S and D, where the path losses are less and thus they contribute more efficiently to the communication process.

V. Conclusion

This paper studied the performance of a generalized system setup, namely, a SISO communication system with multiple RISs and direct path between the source and the destination over the generic κ-μ fading channels. Specifically, it presented tight expressions for the corresponding outage probability, average symbol error probability and ergodic capacity. The considered fading distribution includes most of the widely used fading models. This validates the use of all the derived

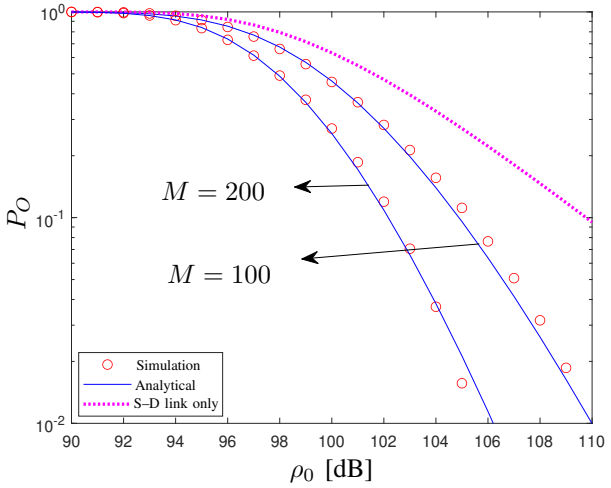

(a) Outage probability, $\rho_{th} = 10$ dB

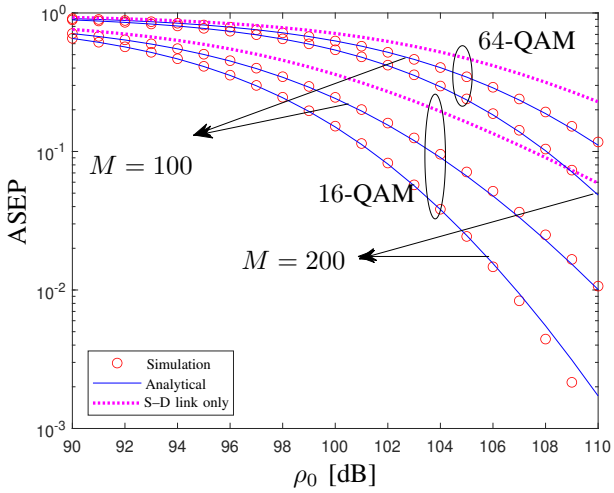

(b) Average symbol error probability

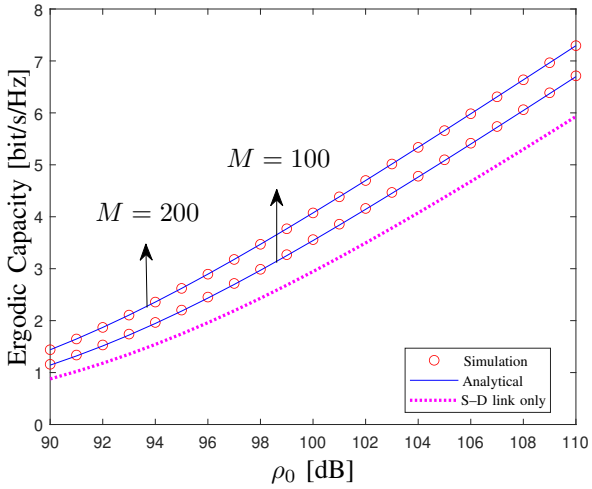

(c) Ergodic capacity

Fig. 3. The outage probability, average symbol error probability and ergodic capacity for different values of M, i.e., the total number of REs.

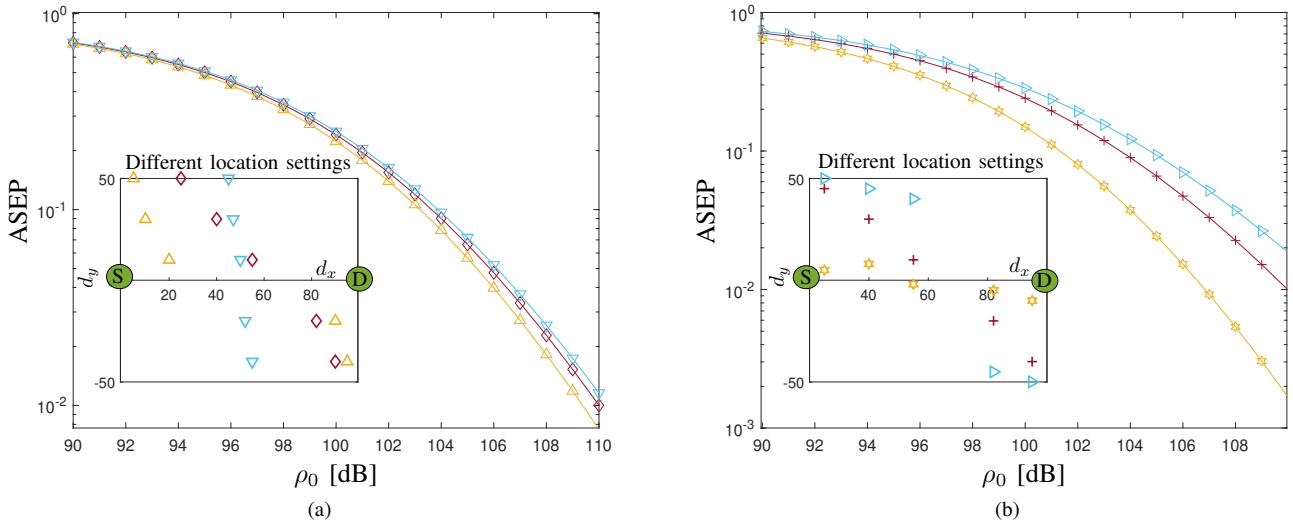

Fig. 4. Impact of the x-position in (a) and the y-position in (b) of the N distributed RISs to the ASEP, while keeping the other dimension's position constant.

expressions for these special cases. The numerical results verified the performed statistical analysis and confirmed the high accuracy of the derived performance measures. Moreover, we showed that increasing the number of reflecting elements equipped on the RISs and placing them closer either to the source or destination, improve the system's performance significantly and increase its diversity gain.

REFERENCES

[1] H. Yang *et al.*, "A programmable metasurface with dynamic polarization, scattering and focusing control," *Sci. Rep.*, vol. 6, Oct. 2016.

[2] N. Kaina, M. Dupré, G. Lerosey, and M. Fink, "Shaping complex microwave fields in reverberating media with binary tunable metasurfaces," *Sci. Rep.*, vol. 4, no. 6693, Oct. 2014.

[3] C. Huang, A. Zappone, G. C. Alexandropoulos, M. Debbah, and C. Yuen, "Reconfigurable intelligent surfaces for energy efficiency in wireless communication," *IEEE Trans. Wirel. Commun.*, vol. 18, no. 8, pp. 4157–4170, Jun. 2019.

[4] Q. Wu and R. Zhang, "Beamforming optimization for intelligent reflecting surface with discrete phase shifts," in *Proc. IEEE Int. Conf. Acoust. Speech Signal Process.*, May 2019, pp. 7830–7833.

[5] C. Pan, H. Ren, K. Wang, W. Xu, M. Elkashlan, A. Nallanathan, and L. Hanzo, "Multicell MIMO communications relying on intelligent reflecting surfaces," *IEEE Trans. Wirel. Commun.*, Jun. 2020.

[6] M. Al-Jarrah, A. Al-Dweik, E. Alsusa, Y. Iraqi, and M.-S. Alouini, "IRS-assisted UAV communications with imperfect phase compensation," *IEEE Trans. Wirel. Commun.*, 2021.

[7] P. Wang, J. Fang, X. Yuan, Z. Chen, and H. Li, "Intelligent reflecting surface-assisted millimeter wave communications: Joint active and passive precoding design," *IEEE Trans. Veh. Technol.*, vol. 69, no. 12, pp. 14 960–14 973, Oct. 2020.

[8] A. Almohamad, A. M. Tahir, A. Al-Kababji, H. M. Furqan, T. Khattab, M. O. Hasna, and H. Arslan, "Smart and secure wireless communications via reflecting intelligent surfaces: A short survey," *IEEE Open J. Commun. Soc.*, vol. 1, pp. 1442–1456, Sep. 2020.

[9] V. C. Thirumavalavan and T. S. Jayaraman, "BER analysis of reconfigurable intelligent surface assisted downlink power domain NOMA system," in *Proc. Int. Conf. on Commun. Syst. Netw.*, Mar. 2020.

[10] M. Badiu and J. P. Coon, "Communication through a large reflecting surface with phase errors," *IEEE Wirel. Commun. Lett.*, vol. 9, no. 2, pp. 184–188, Feb. 2020.

[11] E. Basar, M. Di Renzo, J. De Rosny, M. Debbah, M. Alouini, and R. Zhang, "Wireless communications through reconfigurable intelligent surfaces," *IEEE Access*, vol. 7, pp. 116 753–116 773, Aug. 2019.

[12] D. Kudathanthirige, D. Gunasinghe, and G. Amarasuriya, "Performance analysis of intelligent reflective surfaces for wireless communication," in *Proc. IEEE Int. Conf. Commun.*, Jun. 2020.

[13] A.-A. A. Boulogeorgos and A. Alexiou, "Performance analysis of reconfigurable intelligent surface-assisted wireless systems and comparison with relaying," *IEEE Access*, vol. 8, pp. 94 463–94 483, May 2020.

[14] A. Salhab and M. Samuh, "Accurate performance analysis of reconfigurable intelligent surfaces over Rician fading channels," *IEEE Wirel. Commun. Lett.*, vol. 10, no. 5, pp. 1051–1055, May 2021.

[15] Q. Tao, J. Wang, and C. Zhong, "Performance analysis of intelligent reflecting surface aided communication systems," *IEEE Commun. Lett.*, vol. 24, no. 11, pp. 2464–2468, Nov. 2020.

[16] D. L. Galappaththige, D. Kudathanthirige, and G. Amarasuriya, "Performance analysis of distributed intelligent reflective surface aided communications," in *Proc. IEEE Glob. Commun. Conf.*, Dec. 2020.

[17] L. Yang, Y. Yang, D. B. da Costa, and I. Trigui, "Outage probability and capacity scaling law of multiple RIS-aided networks," *IEEE Wirel. Commun. Letters*, vol. 10, no. 2, pp. 256–260, Feb. 2021.

[18] S. Primak, *Stochastic Methods and Their Applications to Communications: Stochastic Differential Equations Approach*. Wiley, 2004.

[19] M. D. Yacoub, "The κ-μ distribution and the η-μ distribution," *IEEE Antennas Propag. Mag.*, vol. 49, no. 1, pp. 68–81, Feb. 2007.

[20] N. Bhargav and Y. J. Chun, "On the product of two κ-μ random variables and its application to double and composite fading channels," *IEEE Trans. Wireless Commun.*, vol. 17, no. 4, pp. 2457–2470, Apr. 2018.

[21] I. S. Gradshteyn and I. M. Ryzhik, *Table of Integrals, Series, and Products*, 7th ed. Elsevier/Academic Press, 2007.

[22] M. K. Simon and M.-S. Alouini, *Digital Communication over Fading Channels*, 2nd ed. John Wiley and Sons, Inc., Jan. 2005.

[23] I. M. Tanash and T. Riihonen, "Global minimax approximations and bounds for the Gaussian Q-function by sums of exponentials," *IEEE Trans. Commun.*, vol. 68, no. 10, pp. 6514–6524, Oct. 2020.

[24] I. M. Tanash and T. Riihonen, "Coefficients for global minimax approximations and bounds for the Gaussian Q-function by sums of exponentials," Jul. 2020. [Online]. Available: https://doi.org/10.5281/zenodo.4112978